Combined Translation/Pitch Motion: A New Airfoil Dynamic Stall Simulation

D. Favier,* A. Agnes,† C. Barbi,‡ and C. Maresca*
Centre National de la Recherche Scientifique, Marseille, France

The effects of simultaneous velocity and incidence fluctuations on the two-dimensional aerodynamic behavior of a NACA 0012 airfoil are investigated in this paper. A new mechanical system allows driving the airfoil in pitching and in fore and aft motions, as well as in a simultaneous combination of these two basic unsteady motions. In response to the simultaneous velocity and incidence variations, the time-dependent lift and drag fluctuations are measured for increasing values of the reduced frequency and amplitude parameters, including dynamic stall conditions. Complementary information on the dynamic stall occurring in combined motion is provided by skin friction and pressure measurements along the airfoil surface.

Nomenclature

A = amplitude displacement of the airfoil, m
c = airfoil chord, m
C_p = pressure coefficient, $C_p = (p - p_\infty)/(\frac{1}{2}\rho V_\infty^2)$
C_L = lift coefficient, $C_L = L/(\frac{1}{2}\rho V^2 ch)$
C_D = drag coefficient, $C_D = D/(\frac{1}{2}\rho V^2 ch)$
D, L = drag and lift forces, N
f = frequency of oscillation of the airfoil, Hz
h = span of the airfoil, m
k = reduced-frequency parameter, $k = c\omega/2V_\infty$
p, p_∞ = static pressure on the airfoil and at infinity, Pa
t = time, s
V_∞, V = freestream and instantaneous velocities, m/s
x, y = system of coordinates defined in Fig. 2
x_T, y_N = system of coordinates attached to the airfoil chord defined in Fig. 2
α_0, α = mean and instantaneous incidences, deg
$\Delta\alpha$ = amplitude of incidence variations, deg
λ = reduced amplitude of velocity variations, $\lambda = A\omega/V_\infty$
ν, ρ = kinematic viscosity and air density, N/(m · s) and kg/m^3
τ, τ_{st} = unsteady and steady shear stress on the airfoil
ω = pulsation of oscillation, rad/s
ωt = phase of the period, deg

Subscripts

b, t = relative to the upper-side bubble or the stalling vortex
T, N = tangential and normal to the airfoil chord
ss = relative to static stall
st, qst = relative to steady or quasisteady flow conditions

Introduction

AIRFOIL dynamic stall has received considerable attention during the last decade (see Refs. 1–24); it remains, however, a challenging and unsolved problem for both numerical and experimental aerodynamicists.

The unsteady features associated with the dynamic stall process are significant in a variety of specific current aeronautical applications including fixed wings of aircraft, rotary wings of propellers, helicopter rotors, wind-turbine energy conversion systems, blades in cascades of turbomachines, rapid pullup maneuvering on fighter planes, etc. One additional, typical example can also be found in some aquatic wildlife, as dolphin or grampus, that are taking advantage of some specific unsteady motions, on part of their body, to generate complex stalling mechanisms and produce propulsion and high-lift vortex generation.

More generally, dynamic stall features are significant in all applications involving a lifting surface motion where unsteady flow separation occurs owing to instantaneous velocity and/or incidence fluctuations.

Thus, the unsteady stall effects generated on a helicopter's retreating blade have been extensively investigated in past years due to their relevance in the prediction of either local aerodynamic behaviors along the blade span or overall performance of the rotating disk.

Although a proper simulation of the complex rotor blade environment requires considering simultaneous velocity and incidence fluctuations of the oncoming airstream, compressible effects, three-dimensional unsteadiness, oscillating shock waves, etc., most studies have tackled the problem by separating the influence of these combined effects. The influence of the previous parameters has been simulated by means of two-dimensional unsteady flows on airfoils oscillating either in pitching[1-9] and in plunging[10-13] motions, or in translation parallel to the freestream direction.[14-16]

From such previous experimental works, a characteristic and well-documented dynamic stall phenomenology has emerged. Basically, the stall phenomenon consists of a typical unsteady separation-reattachment boundary-layer process that strongly affects the time-dependent lift, drag, and pitching moment behaviors. The airfoil response is also shown[1-16] to be influenced by several parameters (such as airfoil history motion, airfoil shape, oscillation frequency, amplitude of pitch rates, etc.).

In this comprehensive manner, theoretical studies (see e. g., Refs. 17–19) have also been conducted for modeling the unsteady stall events (Euler, Navier-Stokes equations at low and moderate Reynolds number), but some difficulties still remain, especially in modeling the unsteady separation; thus, the generation of unsteady vortices exists.

Presented as Paper 87-1242 at the AIAA 19th Fluids Dynamics, Plasma Dynamics and Laser Conference, Honolulu, HI, June 8–10, 1987; received July 28, 1987; revision received Oct. 29, 1987.

*Senior Research Scientist, Institut de Méchanique des Fluides. Member AIAA.
†Research Engineer, Institut de Méchanique des Fluides.
‡Research Scientist, Institut de Méchanique des Fluides.

Very few studies[20-23] have been devoted to the effects of combining simultaneous velocity and incidence fluctuations on the dynamic stall process as it occurs in the real flow around the rotor blade.

Within this scope, previous works[21-23] were carried out at Institut de Méchanique des Fluides de Marseille (IMFM) by means of an oblique oscillation coupling the variations of velocity V and incidence α around the airfoil. However, this motion was then restricted to sinusoidal V and α variations and to only two combination modes (in-phase and out-of-phase oscillations of V and α).

The present study is an extension of the work along the directions of Refs. 21-23, which aimed to investigate the airfoil aerodynamic behavior generated by arbitrary, periodic V and α fluctuations (sinusoidal or nonsinusoidal). To this end, a new electromechanical oscillating device capable of producing a combined translation-pitch airfoil motion has been designed and realized at IMFM.

In the following sections, the oscillating mechanism and experimental conditions are first described. Emphasis is placed on comparisons of the lift and drag measurements obtained in pure velocity, pure incidence, and combined fluctuations below and through stall. Measurements of skin friction and pressure coefficients are added in some typical cases. The effect of increasing the reduced-frequency parameter on the airfoil aerodynamic behavior is also discussed.

Combined Translation-Pitch Airfoil Device and Measurement Procedures

The principle of combined airfoil motion in two degrees-of-freedom is given in Fig. 1. The translation in the freestream direction V_∞ is realized by an oscillating frame system (see Refs. 14-16), and a V-eccentric cam produces the time-dependent fluctuations of the relative velocity in the form

$$V = V(\omega t) \tag{1}$$

For the simultaneous incidence variations around the quarter-chord of the airfoil (set at a geometric angle of incidence α_0), the mechanical device includes a second α-eccentric cam as depicted in Fig. 1. The synchronized rotation of the two cams is achieved by a driving belt and allows one to select a lead-lag phase Φ between the two cams' rotation. Additionally, a dual parallelogram configuration allows the uncoupled motions in pitch or translation in the V_∞ direction. This system produces the time-dependent fluctuations of instantaneous incidence in the form

$$\alpha = \alpha(\omega t + \Phi) \tag{2}$$

More generally, the adequate design of the V cam and α cam allows the generation of arbitrary periodic (V, α) fluctuations given by the following Fourier series limited to the fourth order:

$$V(t) = V_\infty + \sum_{n=1}^{4} V_n \cos(n\omega t + \Phi_n^v) \tag{3}$$

$$\alpha(t) = \alpha_0 + \sum_{n=1}^{4} \alpha_n \cos(n\omega t + \Phi_n^\alpha) \tag{4}$$

The amplitude of velocity variations λ, the reduced-frequency parameter k, the mean angle of incidence α_0, and the amplitude of incidence variations $\Delta\alpha$ can be varied in the following ranges:

$$0 \le \lambda \le 1; \quad 0 \le k \le 0.9$$

$$0 \text{ deg} \le \alpha_0 \le 20 \text{ deg}; \quad 0 \text{ deg} \le \Delta\alpha \le 15 \text{ deg}$$

The phase shift Φ between the two motions can be varied from 0 to 360 deg.

From Eqs. (3) and (4), it can be seen that a large variety of periodic (V, α) fluctuations can be generated by means of this combined airfoil motion. It is particularly powerful for comparisons to have the ability of the present driving mechanism to pass from one type of motion to another just by setting or removing a belt and to keep the rest of the facility (model, transducers, data-acquisition system, etc.) exactly the same. The device has been also applied to duplicate the cycle of simultaneous V and α variations encountered by a given rotor blade section during the complete rotation at a fixed advancing rotor parameter. The unsteady aerodynamic definition and performance of this blade section are then deduced from wind-tunnel measurements on C_L, C_D, C_M corresponding to the prescribed periodic cycle of (V, α) fluctuations.

The aforementioned mechanical device is designed to fit beneath the test-section floor of the S2-IMFM subsonic wind tunnel (rectangular test section 0.5×1 m^2; length 3 m). The freestream velocity is varied from 2.5 to 25 m/s, providing a Reynolds number range based on the model chord $5 \times 10^4 \le Re_{st} \le 4 \times 10^5$.

The tested airfoil consists of a rectangular wing spanning vertically the entire test section ($h = 0.495$ m; $c = 0.3$ m), with a NACA 0012 profile of static stall incidence $\alpha_{ss} = 12$ deg. The wing is supported in a vertical position and attached to the oscillating system by a single support shaft located at the quarter-chord axis of the model. Measurements of the airfoil aerodynamics coefficients are carried out by means of torsion dynamometers, which are dynamically calibrated. Operating procedures can be found in Refs. 14-16 and 21-23.

Because the torsion dynamometer is directly attached to the airfoil chord, the lift and drag are measured in the (x_T, y_N) system of coordinates (Fig. 2). Therefore, it is necessary to measure both L_N and D_T to obtain one of the two components L or D in the instantaneous system of coordinates (x, y) defined in Fig. 2. Lift L and drag D are then harmonically analyzed to yield the time-averaged value and the four Fourier harmonics in the following way:

$$L = L_0 + \sum_{n=1}^{4} L_n \cos(n\omega t + \Phi_n^L) \tag{5}$$

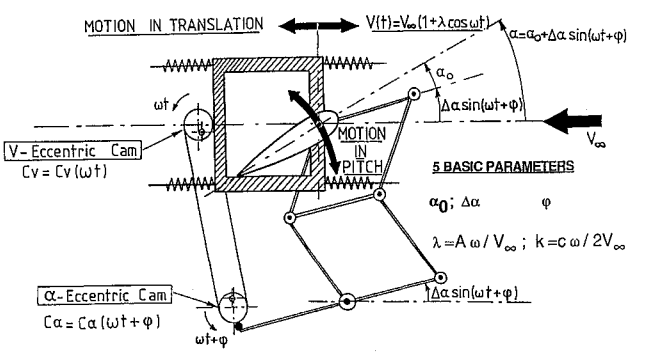

Fig. 1 Combined motion airfoil mechanical principle.

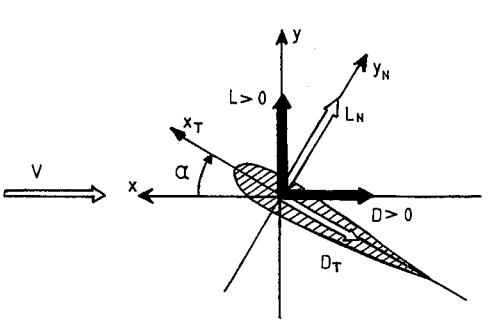

Fig. 2 Systems of coordinates attached to the airfoil (x_N, y_N) and to the instantaneous flow (x, y).

$$D = D_0 + \sum_{n=1}^{4} D_n \cos(n\,\omega t + \Phi_n^D) \tag{6}$$

For the present combined motion tests, the measurement of the instantaneous lift and drag can be performed either in the freestream of the wind tunnel or in a vacuum enclosure surrounding the model in order to eliminate all the contributions other than aerodynamic effects. The aerodynamic quantity G to be measured is then given by the difference

$$G = G_{\text{air}} - G_{\text{vacuum}} \tag{7}$$

Where G_{air} and G_{vacuum} represent the same quantity, respectively, measured on the airfoil oscillating in air and in vacuum. Using this procedure, the instantaneous lift and drag are measured with a percentage error less than 2% (less than 1% for steady mean values).

Moreover, skin friction and pressure distributions along the upper and lower airfoil sides are performed by means of miniature hot-film gauges and pressure transducers (ENDEVCO 8507-2) mounted[15] flush on the skin airfoil surface.

In the present study, the V and α cams generate V and α sinusoidal fluctuations (Fig. 1) in the form

$$V(t) = V_\infty\,(1 + \lambda \cos \omega t) \tag{8}$$

$$\alpha(t) = \alpha_0 + \Delta\alpha \sin(\omega t + \Phi) \tag{9}$$

Thus, the combined airfoil motion experiment is fully defined by the five parameters α_0, $\Delta\alpha$, λ, k, Φ. In fore and aft motion, $\Delta\alpha$ is zero, whereas in pitching motion λ is zero.

In this paper, two selected values of α_0 are specifically investigated: the first one below stall ($\alpha_0 = 6$ deg) and the second one through stall ($\alpha_0 = 12$ deg). For each value of α_0, the time-dependent lift and drag are measured in fore and aft, pitching and combined motion for three couples of λ and k values keeping a ratio $\lambda/k = 1.13$

$$\lambda = 0.114,\ k = 0.101; \quad \lambda = 0.237,\ k = 0.209;$$

$$\lambda = 0.356,\ k = 0.314;$$

In pitching and combined motion $\Delta\alpha$ is constant and equal to 6 deg.

Pure Velocity Fluctuations' Influence (Fore and Aft Airfoil Motion)

Below stall, for $\alpha_0 = 6$ deg, the lift responds to pure velocity fluctuations in a quasisteady way for the values of λ and k considered, as shown in Fig. 3. There is no separation through the cycle that may distort the quasisinusoidal waveform of

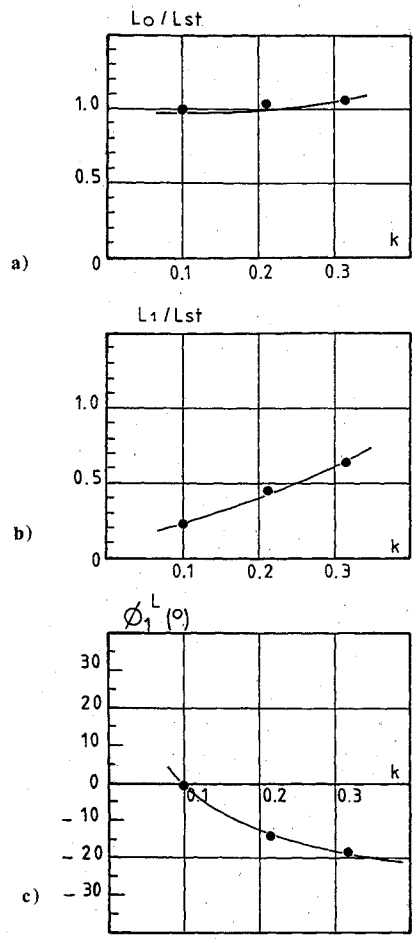

Fig. 4 Lift coefficient ratio L/L_{st} as a function of k for $\alpha_0 = 6$ deg, $\Delta\alpha = 0$ deg, $\lambda/k = 1.13$. a) L_0/L_{st}, b) L_1/L_{st}, c) Φ_1^L.

o	λ = 0.114 k = 0.101	I
+	λ = 0.237 k = 0.209	II
✱	λ = 0.356 k = 0.314	III

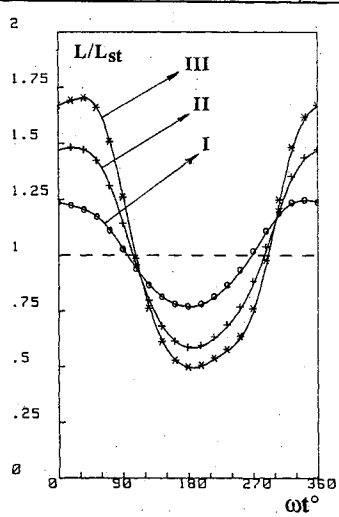

Fig. 3 Lift ratio L/L_{st} as a function of ωt for $\alpha_0 = 6$ deg, $\Delta\alpha = 0$ deg.

o	λ = 0.114 k = 0.101	I
+	λ = 0.237 k = 0.209	II
✱	λ = 0.356 k = 0.314	III

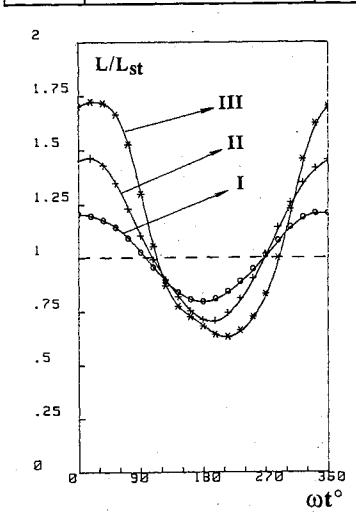

Fig. 5 Lift ratio L/L_{st} as a function of ωt for $\alpha_0 = 12$ deg, $\Delta\alpha = 0$ deg.

the lift, even for values of the reduced parameters λ and k up to 0.3.

The influence of the reduced frequency on the lift ratio L/L_{st} (Fig. 4a) reveals a moderate effect that is well represented by the use of the quasisteady expression[15,16]

$$(L/L_{st})_{qst} = [1 + \lambda \cos(\omega t)]^2 \tag{10}$$

Because λ/k equals 1.13 in these experiments, the increase of L_1/L_{st} is proportional to k (Fig. 4b). The first harmonic phase angle Φ_1^L decreases significantly with λ and k as shown in Fig. 4c.

Through stall, when the airfoil is set at the static angle $\alpha_0 = 12$ deg, a net gain of lift is observed as k increases (see Fig. 5). When λ and k are above 0.3 and the instantaneous velocity is below the mean value V_∞ (90 deg $< \omega t <$ 270 deg), the lift does not drop as much as at lowest incidences. Therefore, a significant increase in the mean lift compared to the static value is observed (Fig. 6a). The first harmonic phase angle Φ_1^L again indicates a significant delay of the lift that increases with k.

From the foregoing results obtained below and through stall, it can be emphasized that pure velocity fluctuations around the airfoil set at fixed α_0 have the following major effects: increasing the mean lift value L_0 over the period, increasing the amplitude L_1 of the lift fluctuations, and delaying the lift first harmonic phase Φ_1^L. For parameters λ and k up to 0.3, these effects involve a quasisteady airfoil behavior at low α_0 (without stall) and a significant unsteady airfoil behavior at high α_0 (through stall).

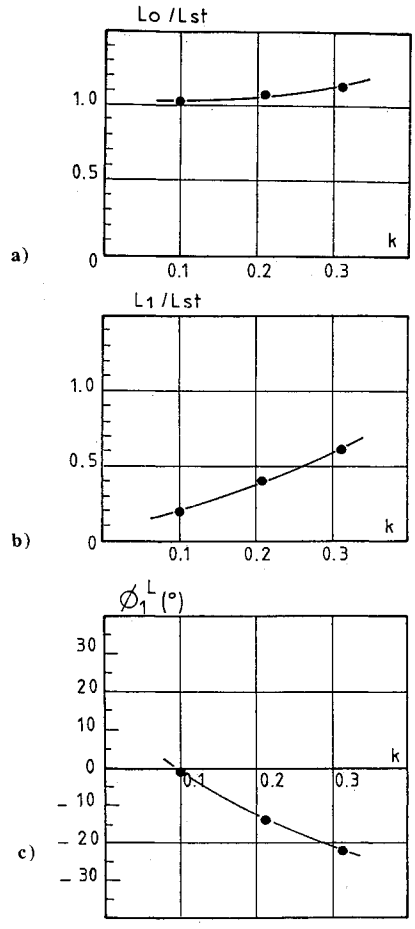

Fig. 6 Lift coefficient ratio L/L_{st} as a function of k for $\alpha_0 = 12$ deg, $\Delta\alpha = 0$ deg, $\lambda/k = 1.13$. a) L_0/L_{st}, b) L_1/L_{st}, c) Φ_1^L.

Pure Incidence Fluctuations' Influence (Pitching Airfoil Motion)

The velocity is now constant, with the airfoil motion a pure incidence variation around the quarter-chord of amplitude $\Delta\alpha = 6$ deg. Figures 7a-c show how the reduced frequency k influences the lift coefficient C_L below stall ($\alpha_0 = 6$ deg). On these figures the static values of C_L (dotted lines) are also presented. For the increasing values of α, the three C_L curves have a slope $dC_L/d\alpha$ nearly equal to the static one $dC_{Lst}/d\alpha$. An overshoot of the maximum static value is experienced in all cases, this effect being accentuated as k increases. As α decreases, the lift coefficient remains well below the static values, producing a clockwise hysteresis loop and, therefore, a net loss of the mean coefficient value C_{L0} over the period.

This k parameter influence is clearly depicted by the mean and first harmonic terms of the lift coefficient plotted as a function of k in Figs. 8a-c. The mean to steady lift coefficient ratio C_{L0}/C_{Lst} appears to remain lower than 1 (Fig. 8a). Increasing the reduced-frequency parameter induces an increase of both the mean ratio C_{L0}/C_{Lst} and fluctuation ratio C_{L1}/C_{Lst}. The first harmonic phase angle $\Phi_1^{C_L}$ between the lift coefficient and the incidence is shown in Fig. 8c, and exhibits a significant increase at the highest value of the frequency parameter ($\Phi_1^{C_L} = 25$ deg at $k = 0.314$).

Figure 9 illustrates the dynamic stall regime. In Fig. 9a, $\alpha_0 = 12$ deg, $\Delta\alpha = 6$ deg, and the sequence of the dynamic stall process is exemplified for $k = 0.1$. As α increases from 6 to 12 deg (where $\alpha_{ss} = 12$ deg is the value of the static stall angle), the unsteady lift coefficient remains close to the static values. Then, a vortex rapidly forms on the upper surface and moves downstream. This modifies the slope of the lift coefficient curve ($\alpha > 12$ deg) and generates the lift coefficient increase above the static values up to the point that the vortex nearly reaches the trailing edge ($\alpha \approx 18$ deg). Then, the lift coefficient drops abruptly. Because α decreases during this part of the

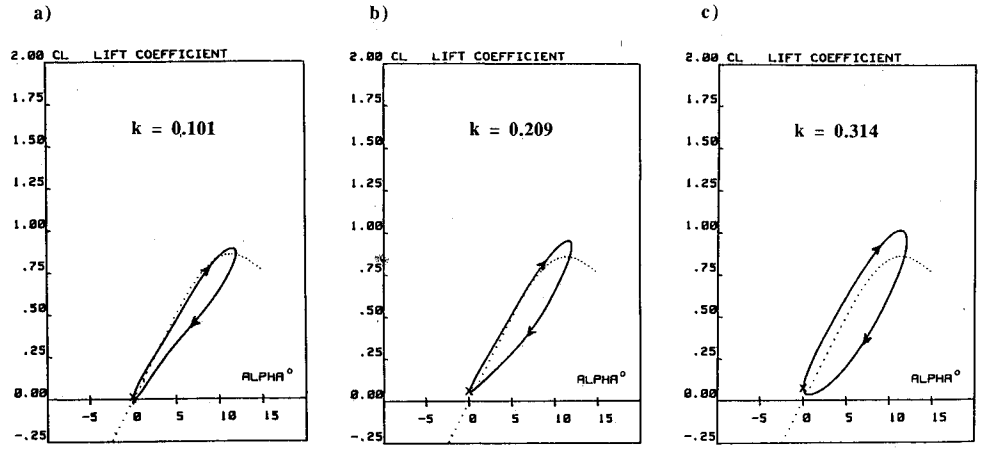

Fig. 7 Lift coefficient C_L as a function of α for $\alpha_0 = 6$ deg, $\Delta\alpha = 6$ deg.

period, the reattachment process occurs next to bring back the lift coefficient at the steady levels.

The reduced-frequency parameter k affects this sequence and particularly influences the reattachment process as illustrated in Figs. 9b-c. When $k = 0.209$ (Fig. 9b), the drop of lift is more severe, the reattachment process is not initiated during the decrease of α, and the lift coefficient does not fully recover the static values when α increases.[24] When $k = 0.314$ and $\alpha > 12$ deg (Fig. 9c), this effect on the slope of the lift coefficient curve is more accentuated.

Figure 10 shows the frequency parameter influence on the mean and first harmonic terms of the lift coefficient during stall. The mean ratio C_{L0}/C_{Lst} behaves as previously observed below stall; however, it slightly exceeds one for high values of k. The values of C_{L1}/C_{Lst} are below those obtained for $\alpha_0 = 6$ deg; however, the increase of C_{L1}/C_{Lst} with k is more important through stall. In Fig. 10c, the first harmonic phase angle behavior is the opposite: an increase was noted below stall, whereas $\Phi_1^{C_L}$ decreases with k for $\alpha_0 = 12$ deg.

Thus, the major effects involved in pure incidence fluctuations around the pitching airfoil in the uniform flow V_∞ consist of a mean lift coefficient slightly below the static one (except at high values of k) and an important increase of C_{L1}/C_{Lst} with the reduced-frequency parameter. As compared to velocity fluctuations, the incidence fluctuations induce quite a different result on the first harmonic phase angle

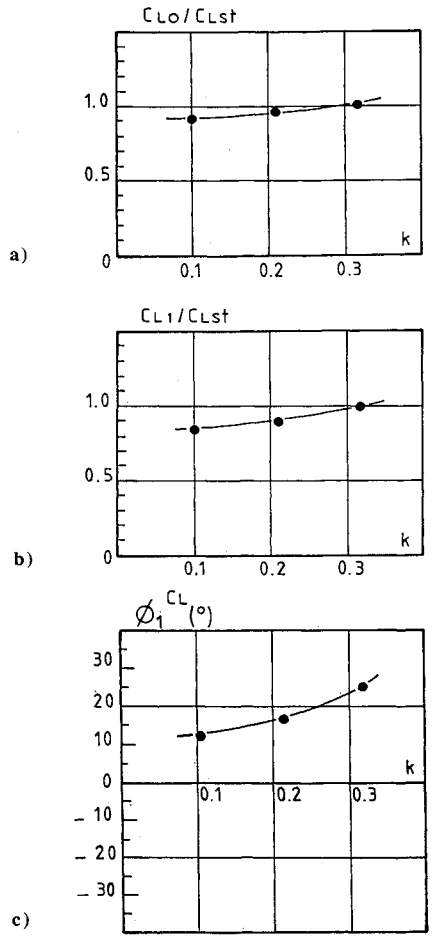

Fig. 8 Lift coefficient ratio C_L/C_{Lst} as a function of k for $\alpha_0 = 6$ deg, $\Delta\alpha = 6$ deg, $\lambda = 0$. a) C_{L0}/C_{Lst}, b) C_{L1}/C_{Lst}, c) $\Phi_1^{C_L}$.

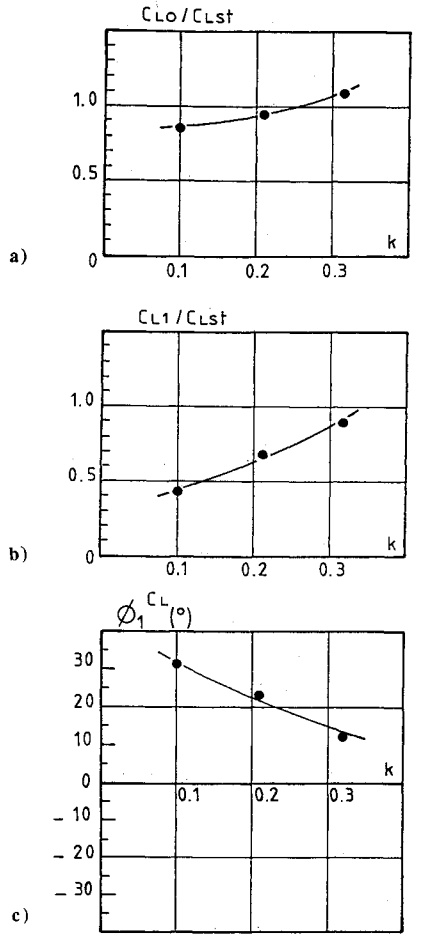

Fig. 10 Lift coefficient ratio C_L/C_{Lst} as a function of k for $\alpha_0 = 12$ deg, $\Delta\alpha = 6$ deg, $\lambda = 0$. a) C_{L0}/C_{Lst}, b) C_{L1}/C_{Lst}, c) $\Phi_1^{C_L}$.

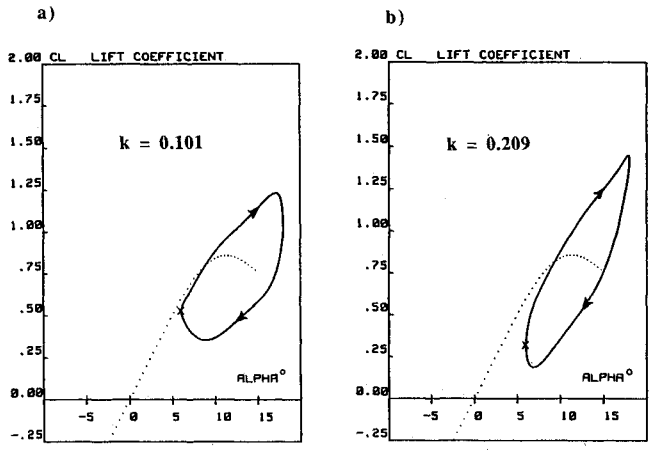

Fig. 9 Lift coefficient C_L as a function of α for $\alpha_0 = 12$ deg, $\Delta\alpha = 6$ deg.

behavior below stall and through stall, since $\Phi_1{}^{C_L}$ increases below stall whereas $\Phi_1{}^{C_L}$ decreases through stall.

Combined Velocity and Incidence Fluctuations' Influence Below Stall

We now consider the combined pitching and fore and aft airfoil motion for two oscillating configurations: in-phase and out-of-phase variations of velocity and incidence. Figure 11 shows an example of simultaneous V and α fluctuations generated with the set of parameters $\alpha_0 = 6$ deg, $\Delta\alpha = 6$ deg, $\lambda = 0.356$, $k = 0.314$ and the two phase shifts $\Phi = 0$ deg, $\Phi = 180$ deg.

Below stall $\alpha_0 = 6$ deg, the corresponding C_L variations are as presented in Figs. 12a–c as a function of the instantaneous incidence α and for three values of k. In these figures, the out-of-phase variations (dashed lines) and in-phase variations (solid lines) are also compared to the static values (dotted lines).

When in-phase variations of V and α are imposed in the airfoil, both the pure velocity and pure incidence influences are present and combined. For low values of λ and k and during the upstroke of α (Figs. 12a and b), the slope of the C_L curves is near the static one as it was in the case of pitch (see the previous section on pure incidence fluctuations influence). However, the C_L values exceed the static ones. In pitch, this was only detected for higher values of λ and k (Fig. 7c).

When $k = 0.314$ (Fig. 12c), a strong unsteady effect is revealed by the modification of the C_L curve, which exhibits a large hysteresis loop that resembles the one obtained during dynamic stall in pitching motion. However, the sharp drop of lift is not present during the α downstroke and suggests that there is only a separation-reattachment bubble occurrence in place of the vortex rolling detected during dynamic stall.

The skin friction measurements confirm these trends well; some evidences of a bubble formation from the leading edge is shown in Fig. 13. The waveforms represent the unsteady shear stress τ over τ_{st} obtained at each x/c gauge location on the upper and lower side of the airfoil. The presence of the bubble on the upper side is clearly revealed by a sharp reduction of the skin friction level ($\tau/\tau_{st} \ll 1$) during part of the period (90 deg $\leq \omega t \leq$ 305 deg for $x/c = 0.12$ and 240 deg $\leq \omega t \leq$ 280 deg for $x/c = 0.8$). The bubble begins to form at the airfoil leading edge and expands slightly beyond the last gauge location ($x/c = 0.8$) on the upper surface at a growing reduced

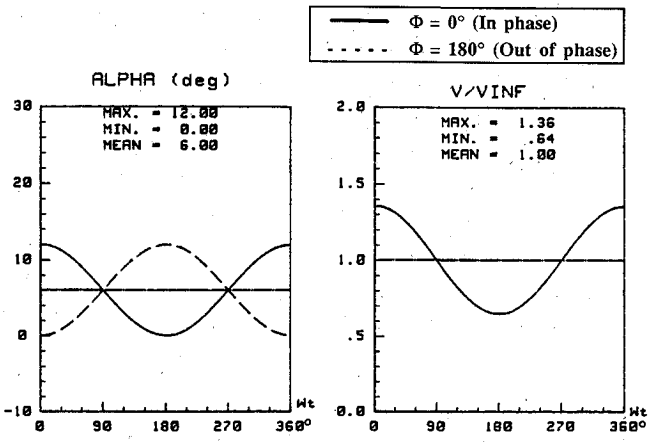

Fig. 11 Example of generation of α and V fluctuations for $\alpha_0 = 6$ deg, $\Delta\alpha = 6$ deg, $\lambda = 0.356$, $k = 0.314$.

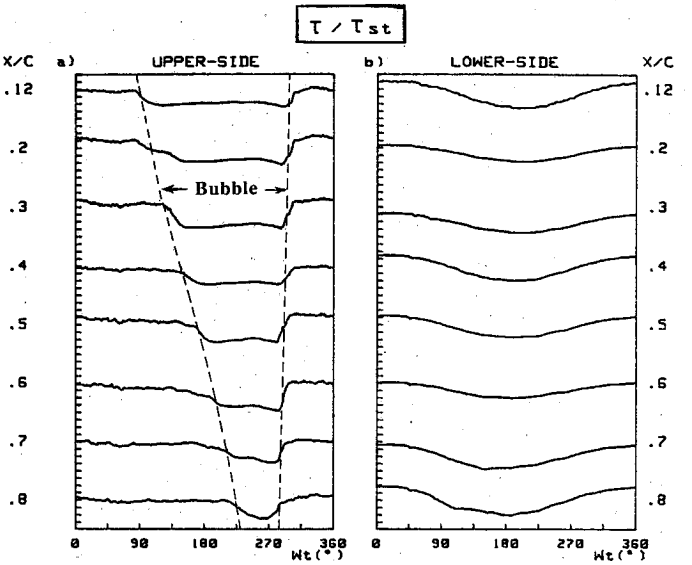

Fig. 13 Skin friction ratio τ/τ_{st} as a function of ωt for $\alpha_0 = 6$ deg, $\Delta\alpha = 6$ deg, $\lambda = 0.356$, $k = 0.314$, $\Phi = 0$ deg (in-phase).

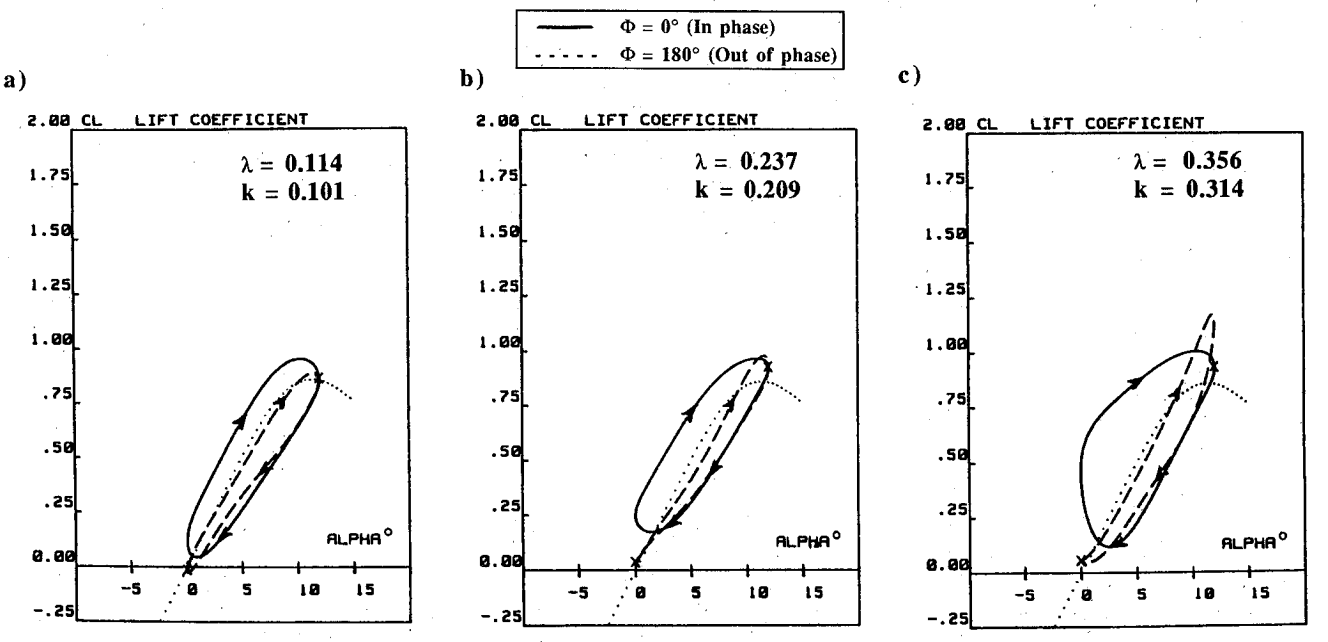

Fig. 12 Lift coefficient C_L as a function of α for $\alpha_0 = 6$ deg, —$\Phi = 0$ deg, ---$\Phi = 180$ deg.

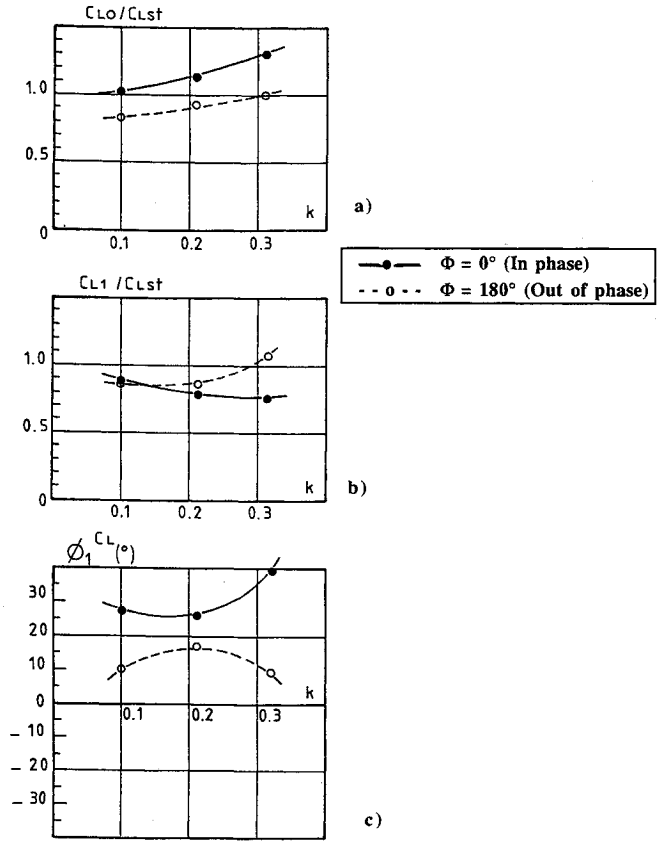

Fig. 14 Lift coefficient ratio C_L/C_{Lst} as a function of k for $\alpha_0 = 6$ deg, $\Delta\alpha = 6$ deg, $\lambda/k = 1.13$. a) C_{L0}/C_{Lst}, b) C_{L1}/C_{Lst}, c) $\Phi_1^{C_L}$.

velocity $V_b/V_\infty = 0.2$ (90 deg $\leq \omega t \leq$ 240 deg); then, it collapses rapidly at $V_b/V_\infty = 1.1$ (280 deg $\leq \omega t \leq$ 305 deg).

When the out-of-phase variations of V and α in Figs. 12a–b are considered at low values of the frequency parameter k, the C_L curves (dashed lines in Figs. 12a–b) are similar to the curves of the pitching motion case (Figs. 7a–b). During the upstroke of α (Figs. 12a–b), the slope of the C_L curves is also close to the static one as was the case in pitch and the C_L values are nearly the static ones. During the downstroke of α (Figs. 12a–b), the out-of-phase and in-phase curves are almost in coincidence. Around $\alpha = 0$ deg, the decrease of the lift coefficient is more significant in the out-of-phase case. At high values of k (Fig. 12c), an important overshoot of the $C_{L\max}$ value is observed, but the gain of lift due to the bubble formation is not detected.

Concerning the mean and first harmonic terms of the lift coefficients, Figs. 14a–c show the influence of the reduced velocity amplitude λ and the frequency parameter k for in-phase and out-of-phase V and α variations below stall. The open symbols are relative to the out-of-phase configuration and the solid symbols to the in-phase configuration.

For out-of-phase oscillations, the C_{L0}/C_{Lst} and C_{L1}/C_{Lst} values compare very well with those obtained in pitching motion (Figs. 14a–b and 8a–b). The out-of-phase lift coefficient behavior is similar to that obtained by pure α variations and indicates the predominance of the α variations' influence in this out-of-phase coupling case. The phase angle $\Phi_1^{C_L}$ appears also to be closely dependent on the frequency and amplitude increase. Because in fore and aft motion, $\Phi_1^{C_L}$ increases (Fig. 4c) and decreases in pitching motion (Fig. 8c), the phase angle does not show a continuous evolution with k in Fig. 14c. The pitchinglike behavior is respected for low values of k, whereas for $k > 0.209$, a decrease of $\Phi_1^{C_L}$ is observed.

For in-phase oscillations, the net gain on the mean value C_{L0}/C_{Lst} shown in Fig. 14a is due to the combined benefit of the velocity and incidence variations. In Fig. 14b, the C_{L1}/C_{Lst} ratio decreases with k even though, in fore and aft motion

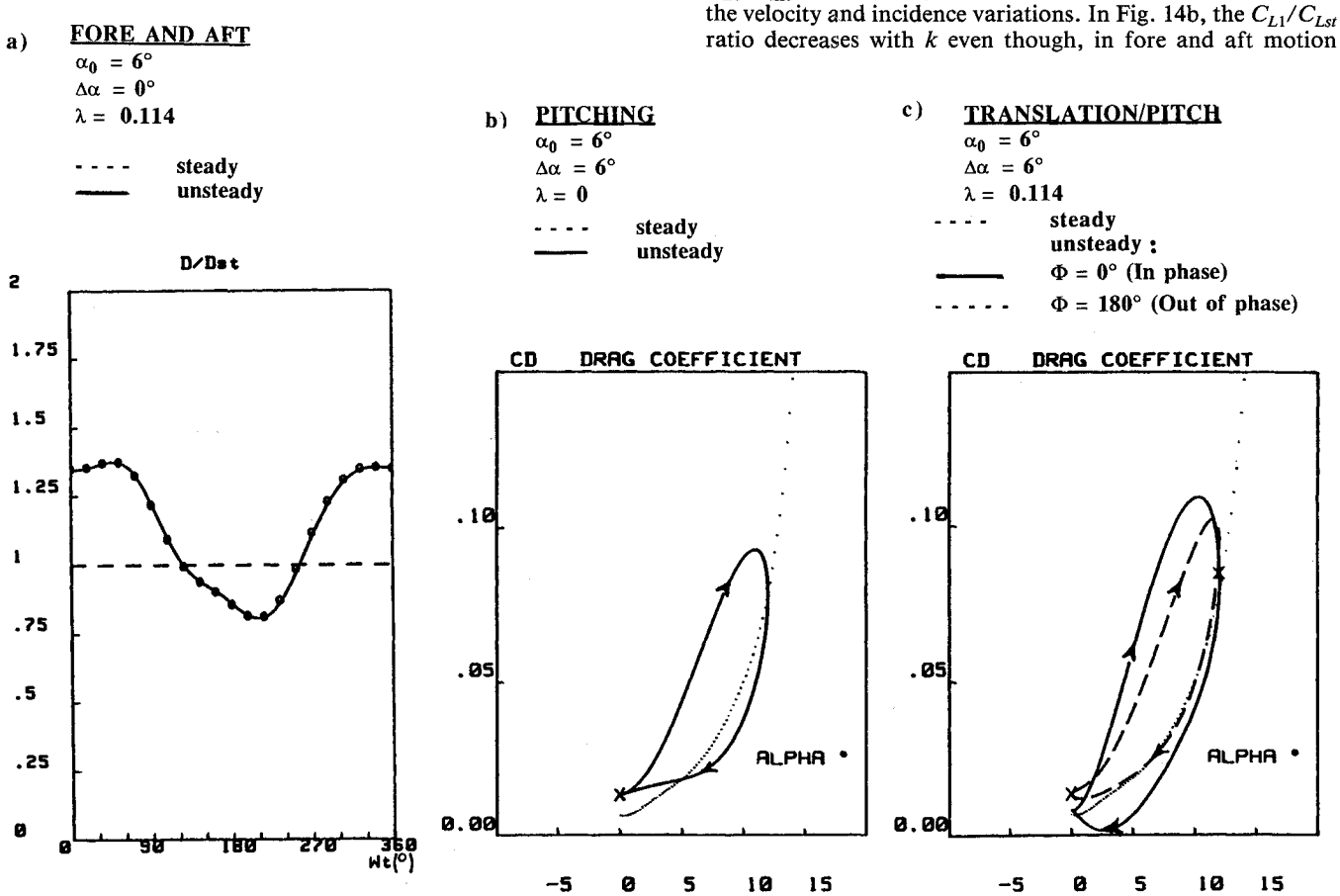

Fig. 15 Drag coefficient for $k = 0.101$: a) $\alpha_0 = 6$ deg, $\Delta\alpha = 0$ deg, $\lambda = 0.114$; b) $\alpha_0 = 6$ deg, $\Delta\alpha = 6$ deg, $\lambda = 0$; c) $\alpha_0 = 6$ deg, $\Delta\alpha = 6$ deg, $\lambda = 0.114$.

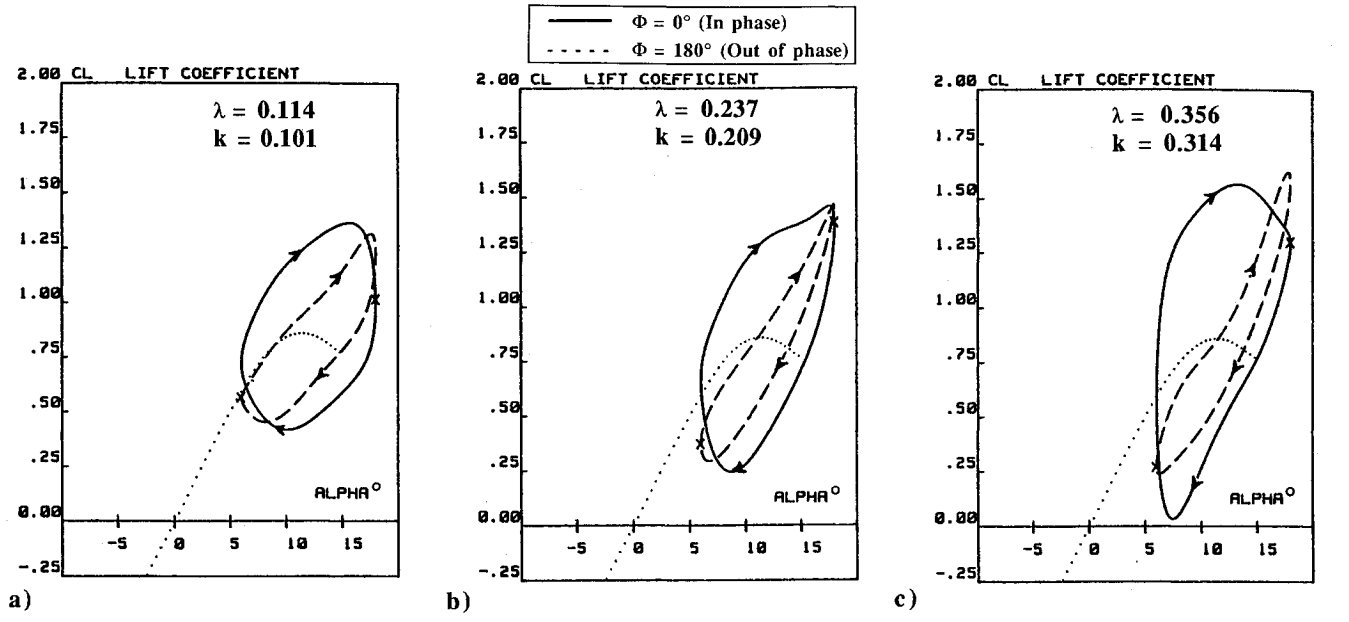

Fig. 16 Lift coefficient C_L as a function of α for $\alpha_0 = 12$ deg, $\Delta\alpha = 6$ deg, —$\Phi = 0$ deg, ---$\Phi = 180$ deg.

(Fig. 4b) and in pitching motion (Fig. 8b), C_{L1}/C_{Lst} is increasing. In Fig. 14c, the behavior of the in-phase and out-of-phase configurations is the opposite. For in-phase variations, $\Phi_1{}^{C_L}$ at first decreases as in the velocity variations case and then increases for $k > 0.209$.

Similar unsteady effects can also be obtained for the drag coefficient behavior C_D. As an example, Fig. 15 gives the instantaneous drag results obtained under the same oscillating conditions at $k = 0.101$ of velocity fluctuations (Fig. 15a), incidence fluctuations (Fig. 15b), and combined fluctuations (Fig. 15c).

For the in-phase variations case, the drag behavior is similar to that due to pure V variations, as previously deduced for the lift coefficient. For pure velocity fluctuations (Fig. 15a), the mean ratio C_{D0}/C_{Dst} equals 1.13; whereas for the in-phase variations, C_{D0}/C_{Dst} equals 1.19, as deduced from Fig. 15c. Moreover, the departure from the static values is observed, as in Fig. 15c, to decrease during all the cycles except for α from 12 to 9 deg. The phase lead between C_D and the V variations appears also to be important ($\Phi_1{}^{C_D} = 35$ deg). If compared to the value obtained for C_L under similar conditions (Fig. 14c), it reveals that the drag drops slightly before the lift does.

In the case of the out-of-phase variations, the C_D behavior is closely similar to that obtained with pure α variations. The drag coefficients C_D plotted in Figs. 15b and 15c lead to coefficients of the Fourier series (C_{D0},C_{D1},$\Phi_1{}^{C_D}$) that compare very well with those of pure α variations. However, in Fig. 15c, the $C_{D\min}$ and $C_{D\max}$ of the out-of-phase curve extend beyond the values measured in the pitching motion. In Figs. 15b and c, for the pitching and out-of-phase configurations, the drag coefficient remains close to the static values for almost all the decreasing values of α and exceeds the static values during the upstroke of α.

Combined Velocity and Incidence Fluctuations' Influence Through Stall

The influence of the combined variations of velocity and indicence is analyzed through stall with α_0 set at 12 deg which coincides with the airfoil static stall incidence ($\alpha_{ss} = 12$ deg). The different trends below stall previously discussed can also be observed on the lift coefficient C_L presented in Figs. 16a–c and appear to be significantly amplified.

When the out-of-phase variations of V and α are considered (dashed lines in Figs. 16a–c), the hysteresis loop is very similar

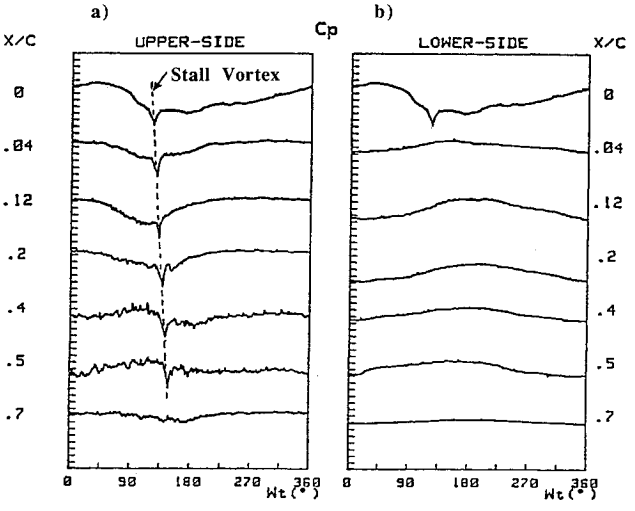

Fig. 17 Pressure coefficient C_p as a function of ωt for $\alpha_0 = 12$ deg, $\Delta\alpha = 6$ deg, $\lambda = 0.114$, $k = 0.101$, $\Phi = 180$ deg (out-of-phase).

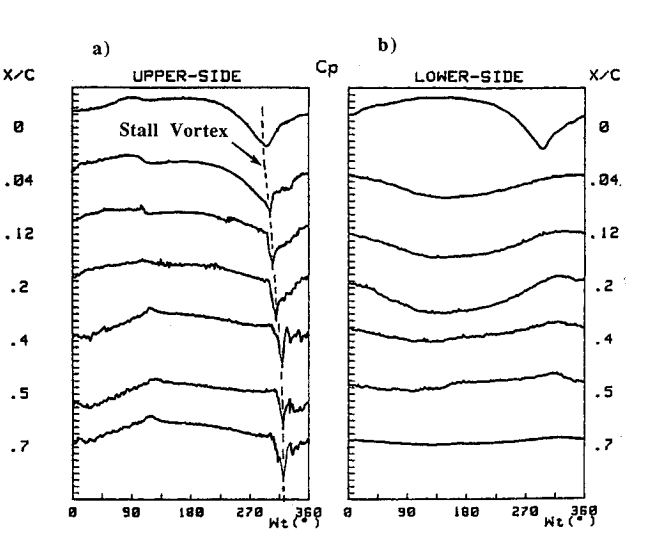

Fig. 18 Pressure coefficient C_p as a function of ωt for $\alpha_0 = 12$ deg, $\Delta\alpha = 6$ deg, $\lambda = 0.114$, $k = 0.101$, $\Phi = 0$ deg (in-phase).

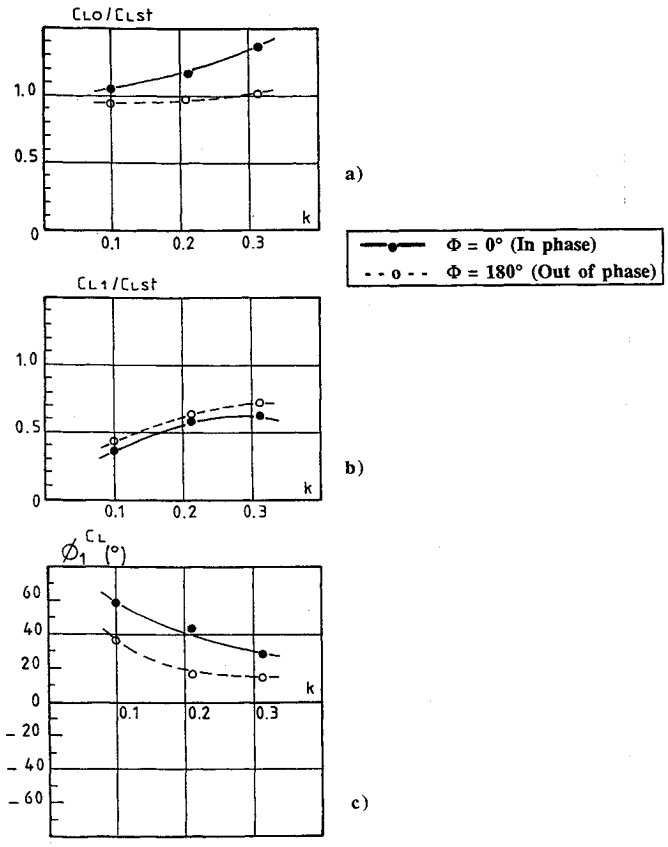

Fig. 19 Lift coefficient ratio C_L/C_{Lst} as a function of k for $\alpha_0 = 12$ deg, $\Delta\alpha = 6$ deg, $\lambda/k = 1.13$. a) C_{L0}/C_{Lst}, b) C_{L1}/C_{Lst}, c) $\Phi_1^{C_L}$.

to the one observed with pure α variations, especially for $k = 0.101$ in Figs. 16a and 9a. In this case, the sequence of dynamic stall events appears to be identical. During the α upstroke, the vortex formation and its propagation along the airfoil change the slope $dC_L/d\alpha$ and increase the lift coefficient C_L above the static values (the C_{Lmax} of the out-of-phase case slightly exceeding the C_{Lmax} of the pitching case). As k increases up to 0.314, C_{Lmax} reaches 1.65 (Fig. 16c).

The time histories of the static pressure coefficients C_p are presented in Fig. 17 for one period to illustrate the vortex rolling along the upper surface of the airfoil. The imprint of the stall vortex is represented by small successive suction peaks that are detected from $x/c = 0$ to $x/c = 0.5$. The vortex appears to convect downstream at a chordwise speed propagation $V_t \approx 0.40\ V_\infty$, which is close to the values usually obtained in the pitching case.[3,5]

When the in-phase variations of V and α are considered (solid lines in Figs. 16a-c), the existence of a quite different type of dynamic stall is revealed in the C_L curves. These curves indeed significantly depart from those obtained in the classical pitching motion case.

During the upstroke of α, the lift coefficient exceeds the static values even for $\alpha < \alpha_{ss}$, a net gain is observed when compared to pure α variations. The increase of V during this part of the period is responsible for these differences. Moreover, the C_{Lmax} and subsequent drop of lift are readily observed (Figs. 16a-c) before the maximum values V_{max} and α_{max} are reached. This indicates that the initiation of the vortex propagation is generated earlier for the in-phase configuration, as also confirmed by the C_p waveforms during stall (Fig. 18), obtained at different transducer locations on the upper and lower side of the airfoil.

From these pressure waveforms corresponding to $k = 0.101$, the vortex propagation is detected from $x/c = 0$ up to $x/c = 0.7$ and around $\omega t = 300$ deg. This compares well with the previous C_L behavior since it is the region of high incidence and velocity values that occurs before the maximum values V_{max} and α_{max} are reached. The intensity of the suction peaks appears also to be more important in the in-phase case than in the out-of-phase case (as it was also obtained for the airfoil oblique motion configuration[23]) and therefore indicates a stronger intensity of the stalling vortex generated during the in-phase stall process. Moreover, the vortex velocity propagation along the chordwise direction appears to be lower for the in-phase configuration ($V_t \approx 0.30\ V_\infty$). The combined effects of earlier vortex initiation, stronger intensity, and lower velocity displacement along the airfoil chord are responsible for the strong unsteady effects observed in C_L behavior (Figs. 16a-c) for the in-phase dynamic stall configuration.

It is also worthy to note that for the two experiments $k = 0.101$ and $k = 0.209$, it is during the upstroke of α that the out-of-phase curve (Figs. 16a-b) and the pitching curve (Figs. 9a-b) are coincident, whereas for the downstroke of α, the in-phase curve (Figs. 16a-b) and the pitching curve (Figs. 9a-b) are coincident. Because both the increase of α and V contribute to increasing the lift, the in-phase variations of the lift coefficient exceed the static and pitching values during the upstroke of α. For similar reasons in the out-of-phase configuration during the downstroke of α, the increase of V effect is opposed to the α decrease effect and, therefore, the lift drop is not as important as it was in pitching motion (Figs. 9a-b). Consequently, the reattachment process is promoted (Fig. 16b) when the in-phase variations of V and α are generated on the airfoil. For the highest value of k ($k = 0.314$), the unsteadiness due to the coupling between velocity and incidence influences becomes more important (Fig. 16c).

Concerning the mean and first harmonic terms of the lift coefficients, Figs. 19a-c summarize the influence of the reduced velocity amplitude λ and the frequency parameter k for in-phase and out-of-phase V and α variations through stall.

For in-phase variations (Fig. 19a), the influence of the velocity fluctuations produces an important increase in the mean ratio (C_{L0}/C_{Lst}). The values of C_{L1}/C_{Lst} shown in Fig. 19b are of the same order obtained in the V variations case (Fig. 6b); they exhibit the same behavior as k increases. The phase angle $\Phi_1^{C_L}$ presented in Fig. 18c decreases as k increases and expresses the important phase lead of the lift with respect to the velocity and incidence fluctuations already noticed in Fig. 16a.

For the out-of-phase variations (open symbols in Fig. 19), the behavior of the lift Fourier series terms is similar to that of the pitching motion terms. It is only for the highest value of k that the mean lift ratio (C_{L0}/C_{Lst}) is above 1. The values of C_{L1}/C_{Lst} shown in Fig. 19b are slightly lower than those obtained in the α variations case (Fig. 10b) and increase with k. The phase angle $\Phi_1^{C_L}$ (Fig. 19c) is below that obtained in the in-phase variations configuration.

Conclusions

The experimental results presented in this paper have been obtained by means of a new unsteady experiment combining the velocity and incidence variations around the airfoil. The unsteady effects due to either pure velocity fluctuations or pure incidence fluctuations and to the combined motion either in-phase or out-of-phase have been compared.

For V and α oscillations below stall and moderate values of the reduced parameters λ and k, the unsteady effects are dominated by the velocity fluctuations when the in-phase case is considered and by the incidence fluctuations for the out-of-phase case. These results confirm very well the conclusions of the tests previously run in airfoil oblique motion.[23]

Moreover from the present experiments, it has been shown that higher values of the reduced parameters $\lambda > 0.3$ and $k > 0.3$ produce a more complex relationship between V and α fluctuations. The skin friction measurements performed in the

in-phase configuration have indeed revealed the formation and development of a leading-edge bubble on the upper side of the airfoil, which appears to be responsible for the net gain of the lift coefficient during the α upstroke as well as the unsteady behavior of the phase-angle-of-lift first harmonic $\Phi_1{}^{C_L}$. On the other hand, the out-of-phase case does not indicate such a bubble formation and influence. Consequently, the lift coefficient exhibits a behavior more similar to that obtained in pitching motion.

These results obtained below stall should stimulate an effort to predict numerically the flowfield around an airfoil in the combined motion. This implies that one must take into account the nonlinear behavior induced by both the unsteady boundary-layer effects and the inviscid-viscid interaction generated by the coupling of V and α.

For V and α oscillations through stall, the predominant effect of V in the in-phase configuration as well as the predominant α influence for the out-of-phase configuration has also been shown. A quite different dynamic stall process has been exemplified in the two coupling configurations. For the in-phase configuration, the simultaneous increase of the velocity and incidence, during the α upstroke, significantly modifies the vortex development (initiation, intensity, chordwise propagation velocity) and induces a lift hysteresis different from that obtained in pure velocity or incidence fluctuations. For the out-of-phase configuration, the combined velocity and incidence influence produce a milder unsteady effect on the lift coefficient behavior and the associated stalling vortex. This dynamic stall process remains similar to the one generated by the classical pitching motion.

For the in-phase and out-of-phase configurations, the influence of the increase of the parameters λ and k is dominated by the response of each dynamic stall process. This influence consists of an increase in the mean lift coefficient C_{L0} (more accentuated for the in-phase coupling) an increase of the first harmonic lift C_{L1}, and a decrease of the phase angle $\Phi_1{}^{C_L}$.

Acknowledgment

This work was supported by the Service Technique des Programmes Aéronautiques under Grant 86-95011.

References

[1]McCroskey, W. J., Carr, L. W., and McAlister, K. W., "Dynamic Stall Experiments on Oscillating Airfoils," *AIAA Journal,* Vol. 14, June 1976, pp. 57–63.

[2]McCroskey, W. J., "Some Current Research in Unsteady Fluid Dynamics," 1976 Freeman Scholar Lecture, *ASME Journal of Fluids Engineering,* Vol. 12, March 1977, pp. 8–39.

[3]Carr, L. W., McAlister, K. W., and McCroskey, W. J., "Analysis of Dynamic Stall Based on Oscillating Airfoils Experiments," NACA TND-8382, Jan. 1977; also NASA TP-1100, Jan. 1978.

[4]McCroskey, W. J., McAlister, K. W., Carr, L. W., Pucci, S. L., Lambert, O., and Indergand, R. F., "Dynamic Stall on Advanced Airfoil Sections," *Journal of American Helicopter Society,* Vol. 26, July 1981, pp. 40–50.

[5]McCroskey, W. J., "The Phenomenon of Dynamic Stall," NASA TM-81264, March 1981.

[6]Ham, N. D., "Some Recent MIT Research on Dynamic Stall," *Journal of Aircraft,* Vol. 9, May 1972, pp. 378–379.

[7]Parker, A. G., "Force and Pressure Measurement on an Airfoil Oscillating through Stall," *Journal of Aircraft,* Vol. 13, Oct. 1976, pp. 823–827.

[8]Ericsson, L. E. and Reding, J. P., "Unsteady Airfoil Stall: Review and Extension," *Journal of Aircraft,* Vol. 8, Aug. 1971, pp. 606–616.

[9]Ericsson, L. E. and Reding, J. P., "Quasi-Steady and Transient Dynamic Stall Characteristics," Paper No. 24, AGARD CP204, Feb. 1977.

[10]Carta, F. O., "A Comparison of Pitching and Plunging Response of an Oscillating Airfoil," NASA CR-3172, Oct. 1979.

[11]Favier, D., Maresca, C., and Rebont, J., "Profil d'Aile à Grande Incidence en Mouvement de Pilonnement," *Proceedings of the 16th Colloquium of Applied Aerodynamics,* Association Aéronautique et Astronautique de France, Lille, France, Nov. 1979, pp. 1–21.

[12]Ericsson, L. E. and Reding, J. P., "The Difference Between the Effects of Pitch and Plunge on Dynamic Airfoil Stall," *Proceedings of the 9th European Rotorcraft Forum,* Paper No. 9, Stresa, Italy, Sept. 1983.

[13]Ericsson, L. E. and Reding, J. P., "A Critical Look at Dynamic Simulation of Viscous Flow," Paper No. 6, AGARD CP 836, May 1985.

[14]Rebont, J., Maresca, C., Favier, D., and Valensi, J., "Recollement Dynamique sur un Profil d'Aile en Movement de Tamis: Influence des Paramètres d'Oscillaltion," Paper No. 29, AGARD CP 227, Sept. 1977.

[15]Maresca, C., Favier, D., and Rebont, J., "Experiments on an Aerofoil at High Angle of Incidence in Longitudinal Oscillations," *Journal of Fluid Mechanics,* Vol. 92, Part 4, June 1979, pp. 671–690.

[16]Favier, D., "Aérodynamique Instationnaire d'un Profil d'Aile Soumis à des Variations de Vitesse et d'Incidence," Thèse de Doctorat d'Etat, Université d'Aix-Marseille, France, Oct. 1980.

[17]Tassa, Y. and Sankar, N. L., "Dynamic Stall of an Oscillating Airfoil in Turbulent Flow Using Time Dependent Navier-Stokes Solver," *Proceedings of International Union of Theoretical and Applied Mechanics Symposium,* Toulouse, France, May 1981, pp. 207–220.

[18]Lecointe, Y. and Piquet, J., "Unsteady Viscous Flow Round Moving Circular Cylinders and Airfoils," AIAA Paper 85-1490, July 1985.

[19]Geibler, W., Carr, L. W., and Cebeci, T., "Unsteady Separation Characteristics of Airfoils Operating Under Dynamic Stall Conditions," *Proceedings of the 12th European Rotorcraft Forum,* Garmish, FRG, Paper 32, Sept. 1986.

[20]Saxena, L. S., Fejer, A. A., and Morkovin, M. V., "Effects of Periodic Changes in Free Stream Velocity on Flows over Airfoils near Static Stall," *Nonsteady Fluid Dynamics, Proceedings of the Winter Annual Meeting of American Society of Mechanical Engineers,* Dec. 1978, pp. 111–116.

[21]Favier, D., Rebont, J., and Maresca, C., "Large Amplitude Fluctuations of Velocity and Incidence on an Oscillating Airfoil," *AIAA Journal,* Vol. 17, Nov. 1979, pp. 1264–1267.

[22]Maresca C., Favier, D., and Rebont, J., "Unsteady Aerodynamics of an Airfoil at High Angle of Incidence Performing Various Linear Oscillations in a Uniform Stream," *Journal of the American Helicopter Society,* Vol. 26, April 1981, pp. 40–45.

[23]Favier, D., Maresca, C., and Rebont, J., "Dynamic Stall due to Fluctuations of Velocity and Incidence," *AIAA Journal,* Vol. 20, July 1982, pp. 865–871.

[24]McCroskey, W. J. and Pucci, S. L., "Viscous-Inviscid Interaction on Oscillating Airfoils in Subsonic Flow," AIAA Paper 81-0051, AIAA 19th Aerospace Sciences Meeting, St. Louis, MO, Jan. 1981.